INSTITUTE OF PHYSICS PUBLISHING PLASMA PHYSICS AND CONTROLLED FUSION

Plasma Phys. Control. Fusion **48** (2006) 1749–1763 doi:10.1088/0741-3335/48/12/005

Detection of short-scale turbulence in the next generation of tokamak burning plasma experiments

E Mazzucato

Princeton Plasma Physics Laboratory, Princeton, NJ 08543, USA

E-mail: mazzucato@pppl.gov

Received 20 April 2006, in final form 17 October 2006
Published 6 November 2006
Online at stacks.iop.org/PPCF/48/1749

Abstract
In this paper, we discuss the use of coherent scattering of CO_2 lasers for high resolution measurements of short-scale turbulent fluctuations in the next generation of tokamak burning plasma experiments. The unique feature of the proposed scheme is the oblique propagation of the probing beam with respect to the magnetic field, with the toroidal curvature of field lines playing a major role in improving the spatial resolution of measured signals. In addition, small scattering angles and negligible wave refraction effects minimize the size of needed ports—a matter of vital importance for a plasma diagnostic that must operate in the hostile environment of a burning plasma.

1. Introduction

The direct impact of plasma confinement on the feasibility of an economical fusion reactor makes the investigation of plasma transport one of the most important tasks for the next generation of DT burning plasma experiments—such as IGNITOR and ITER [1, 2]—where for the first time the kinetic energy of charged fusion products will be the dominant source of plasma heating. Consequently, since both theory and experiments suggest that plasma transport in tokamaks exceeds neoclassical values because of the existence of a short-scale turbulence [3, 4], the study of the latter will be of paramount importance for these experiments.

The main difficulty in choosing a method for the measurement of turbulent fluctuations is the scarcity and limitations of available diagnostics. For example, the method of coherent wave scattering, that was so prominent in early fluctuation studies [5–9], has a poor spatial resolution—very often larger than the plasma minor radius. The method of beam emission spectroscopy [10] is sensitive only to relatively large-scale fluctuations, and the negative ion beams required for accessing the main core of a burning plasma are still under development. Likewise, microwave reflectometry can detect only large-scale fluctuations, and the interpretation of signals from the outer plasma region—where turbulent fluctuations are very large—is extremely difficult [11, 12].

Meeting the requirements of plasma diagnostics will be extremely difficult in the next generation of burning plasma experiments, where plasma accessibility will require penetration of not only toroidal magnets and vacuum vessels, as in present experiments, but also of thick insulating layers and radiation shields. Inevitably, only the most simple and reliable diagnostics will survive in such a hostile environment.

Ideally, what is needed is a method capable of detecting all types of short-scale turbulent fluctuations without the need for large ports. This is a daunting task given the variety of fluctuations in tokamak plasmas—from the ion temperature gradient mode (ITG) and the trapped electron mode (TEM), both with the scale of the ion Larmor radius, to the electron temperature gradient (ETG) mode with the scale of the electron Larmor radius [3, 4]. As an example, in ITER [2] with an average plasma temperature of 10 keV and a magnetic field of 5.3 T, the wave number of possible fluctuations varies from 1–2 cm^{-1} for the ITG/TEM modes to 50–100 cm^{-1} for the ETG mode. In IGNITOR [1], because of its high magnetic field (13 T), we expect shorter fluctuations by a factor of $\sim$2.5.

In this paper, we discuss the possibility of employing coherent scattering of CO_2 lasers for localized measurements of turbulent fluctuations in a tokamak burning plasma experiment. This is motivated by some important advantages of this technique, such as the availability of high power single-mode lasers, negligible wave refraction effects and relatively modest requirements for the size of needed ports.

2. Coherent scattering of electromagnetic waves

Coherent scattering of electromagnetic waves is a powerful technique, capable of providing the spectral power of turbulent density fluctuations. It was employed extensively in early studies of plasma turbulence, including the first detection of short-scale turbulence in tokamaks [5, 6].

The process of coherent scattering of electromagnetic waves by turbulent density fluctuations can be characterized by the differential cross section

$$\sigma = (e^2/mc^2)^2 S(\boldsymbol{k}, \omega), \tag{1}$$

where $S(\boldsymbol{k}, \omega)$ is the spectral density of plasma density fluctuations [13]. The frequency (ω) and wave vector ($\boldsymbol{k}$) of fluctuations must satisfy the energy and momentum conservation, i.e. $\omega = \omega_s - \omega_0$ and $\boldsymbol{k} = \boldsymbol{k}_s - \boldsymbol{k}_0$, where superscripts s and 0 refer to scattered and incident waves, respectively. Since for the topic of this paper $\omega_s \approx \omega_0$ and $k_s \approx k_0$, the scattering angle θ must satisfy the Bragg condition

$$k = 2k_0 \sin(\theta/2). \tag{2}$$

The instrumental resolution of scattering measurements is limited by the size of probing and scattered beams, that in this paper we will assume having a Gaussian amplitude profile $A(r_\perp) = \exp(-r_\perp^2/w^2)$, with $r_\perp$ a radial coordinate perpendicular to the direction of propagation and w the beam radius. The wave number resolution of measured fluctuations, then, depends on the beam spectrum $G(\kappa_\perp) = \exp(-\kappa_\perp^2/\Delta^2)$, where $\Delta = 2/w$ and $\kappa_\perp$ is the wave number component perpendicular to the direction of propagation. For example, we get $\Delta \approx 0.7\,\mathrm{cm}^{-1}$ for $w = 3$ cm, which is satisfactory when compared with the wave number of expected fluctuations. However, if we take the size of the common region between the probing and the scattered beam as a measure of spatial resolution (δl), we get $\delta l \approx 2k_0 w/k$, from which one might conclude that it is difficult to perform localized measurements of plasma turbulence with coherent scattering of electromagnetic waves. Fortunately, this estimate is valid only for an isotropic turbulence, which is not the case in tokamak plasmas where short-scale fluctuations satisfy the relation $\boldsymbol{k}\cdot\mathbf{B}/B \approx 1/qR$ [3, 4] (with q the magnetic safety factor

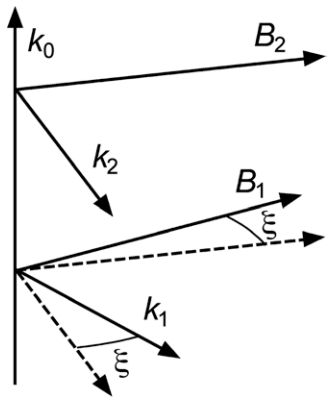

Figure 1. Magnetic field ($\boldsymbol{B}_1$ and $\boldsymbol{B}_2$ and fluctuation wave vector ($\boldsymbol{k}_1$ and $\boldsymbol{k}_2$) at two points of a probing beam ($\boldsymbol{k}_0$) propagating perpendicularly to the magnetic surfaces. Scattering angles are equal (i.e. $k_1 = k_2$) and small (i.e. $\boldsymbol{k}_1$ and $\boldsymbol{k}_2$ are nearly perpendicular to $\boldsymbol{k}_0$).

and R the plasma major radius). For all practical purposes, this can be written as

$$\boldsymbol{k}\cdot\mathbf{B} = 0. \tag{3}$$

In this paper, we will impose this constraint on the range of possible fluctuations, i.e. we will assume the wave vector of plasma fluctuations to be perpendicular to the magnetic field. In this case, then, the spatial variation of the magnetic field direction can modify the instrumental selectivity function by detuning the scattering receiver [9, 14]. This can be easily understood when the probing wave propagates perpendicularly to the magnetic surfaces and scattering angles are small (figure 1). From the beam spectrum $G(\kappa_\perp)$, we can readily obtain the instrumental selectivity function [9]

$$F(\boldsymbol{r}) = \exp[-(2k\sin(\xi(r)/2)/\Delta)^2], \tag{4}$$

where $\xi(r)$ is the change in pitch angles of magnetic field lines starting from the point where scattered waves are detected with maximum efficiency, i.e. from the aiming point of the receiving antenna.

From equation (4), we obtain the spatial resolution $\delta l \approx 2\Delta/k\langle \mathrm{d}\xi/\mathrm{d}r\rangle$, where $\langle \mathrm{d}\xi/\mathrm{d}r\rangle$ is the average derivative of the magnetic pitch angle inside the scattering region. Compared with the above estimate, equation (4) does not depend on the wave number of the probing wave. This is very advantageous for scattering of far infrared waves, since equation (4) gives a spatial resolution that is substantially smaller than the dimension of the common region between the probing and scattered beams. Unfortunately, very often this is not satisfactory because of the small value of $\mathrm{d}\xi/\mathrm{d}r$ in tokamaks, as in the case of the magnetic configuration of figure 2 with the magnetic pitch angle distribution of figure 3. In this case, we get the instrumental selectivity function of figure 4 for fluctuations with a wave number of $2\,\mathrm{cm}^{-1}$ and a probing beam ($w = 3$) propagating on the tokamak mid-plane perpendicularly to the magnetic field. In spite of the fact that such a scattering geometry—indeed very impractical and difficult to implement—maximizes the benefits of magnetic shear, the instrumental selectivity function in figure 4 is very broad and would therefore result in poorly localized measurements.

In this paper, we will consider the general case of a probing beam propagating at an arbitrary angle with the magnetic field [14]. This is motivated by the fact that the conditions for coherent scattering become strongly dependent on the toroidal curvature of magnetic field lines when the probing beam forms a small angle with the magnetic field. This is schematically

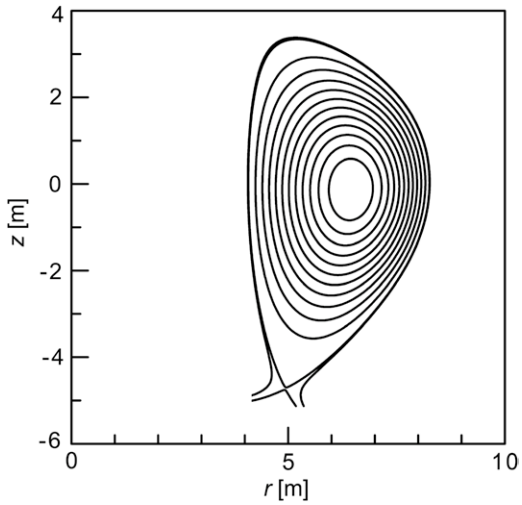

Figure 2. Poloidal cross section of an ITER-like tokamak used throughout the paper for deriving the properties of the proposed scattering scheme.

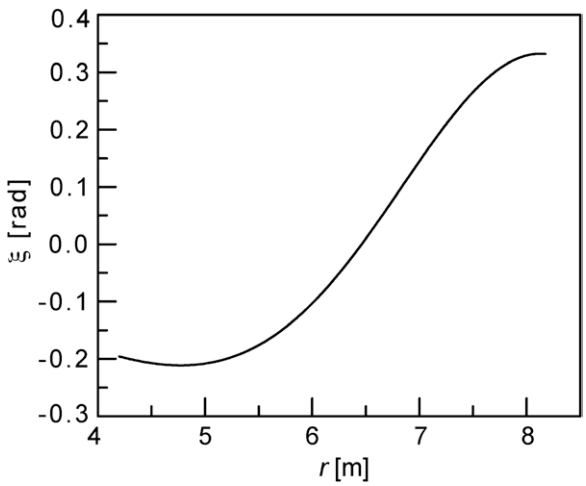

Figure 3. Pitch angle of magnetic field lines on the equatorial plane of the tokamak configuration of figure 2.

illustrated in figure 5, showing a case where the probing beam is on the tokamak mid-plane. For a given fluctuation wave number, the wave vector of the scattered wave ($\boldsymbol{k}_s$) is parallel to the mid-plane only if the wave is scattered at one of the two points P_1 and P_2 (toroidally separated by an angle equal to the scattering angle), where the fluctuation wave vector ($\boldsymbol{k}$) is in the plasma radial direction. At all the other probing locations, then, equations (2) and (3) impose on the scattered wave to propagate at an oblique angle with the mid-plane. It is this phenomenon that we will exploit for localizing the scattering region. As we shall see in the following, its size depends on the spatial distribution of magnetic pitch angles and may become very small in standard tokamak plasmas [14]. Furthermore, we will find that this scattering scheme has the additional advantage of minimizing the radial resolution of fluctuation measurements, i.e. the footprint of the scattering region in the radial plasma direction.

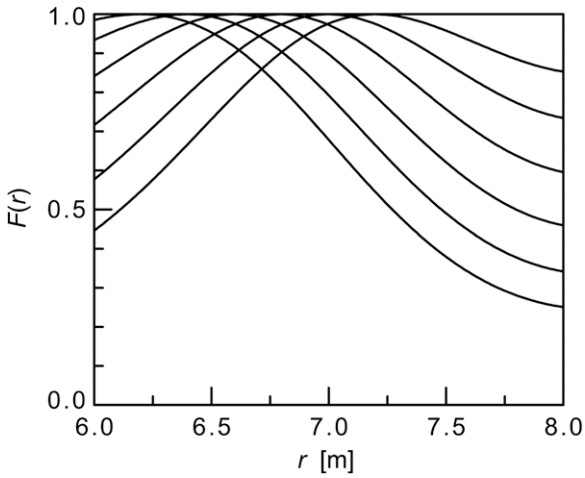

Figure 4. Instrumental selectivity functions for detection of fluctuations with $k = 2\,\mathrm{cm}^{-1}$ at several radial locations. The probing beam has a radius of 3 cm and propagates on the equatorial plane perpendicularly to the magnetic field.

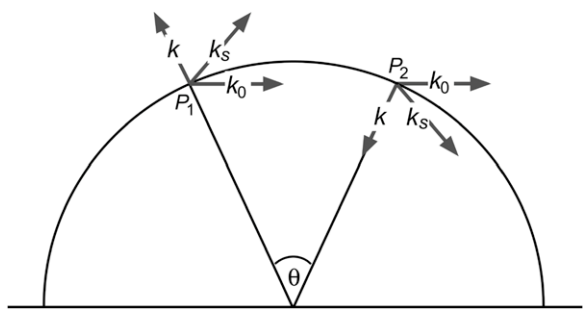

Figure 5. Scattering geometry with the probing beam ($\boldsymbol{k}_0$) on the tokamak mid-plane. For a given fluctuation wave number (k), equations (2) and (3) are satisfied only at P_1 and P_2 (toroidally separated by the scattering angle θ.

3. Instrumental selectivity function

Throughout this paper, we will assess the localization properties of scattering measurements with an instrumental selectivity function—as defined by the collection efficiency of the receiving antenna—which was derived in [14]. For the sake of clarity and reader's convenience, here we summarize its derivation.

In the system of orthogonal coordinates (u, v, t) with the t-axis parallel to $\boldsymbol{k}_0$, we define the polar angle φ with

$$k_{su} = k_0 \sin\theta \cos\varphi, \qquad k_{sv} = k_0 \sin\theta \sin\varphi, \qquad k_{st} = k_0 \cos\theta. \tag{5}$$

Let us now consider scattered waves originating from two points of the probing beam with identical scattering angles but different wave vectors $\boldsymbol{k}_s^1$ and $\boldsymbol{k}_s^2$, respectively (figure 6). From equation (5), we get

$$\frac{\boldsymbol{k}_s^1 \cdot \boldsymbol{k}_s^2}{\boldsymbol{k}_0 \cdot \boldsymbol{k}_0} \equiv \cos\alpha = \cos^2\theta + \sin^2\theta \cos\delta\varphi, \tag{6}$$

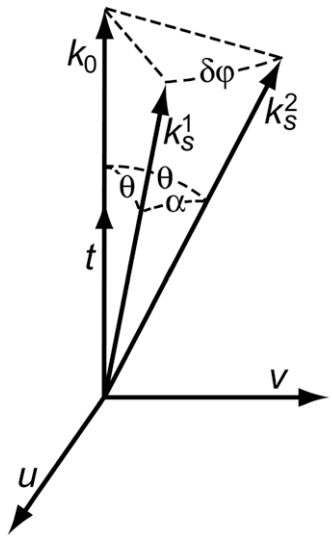

Figure 6. Orthogonal coordinates (u, v, t) with the t-axis along the wave vector of the probing beam ($\boldsymbol{k}_0$).

where $\delta\varphi = \varphi_2 - \varphi_1$, giving

$$\cos\,\alpha = 1 - \sin^2\,\theta(1 - \cos\,\delta\varphi) = 1 - 2\sin^2(\delta\varphi/2)\sin^2\,\theta. \tag{7}$$

For $\theta^2 \ll 1$ (always satisfied in this paper), this becomes

$$\alpha^2 \approx 4\theta^2\sin^2(\delta\varphi/2). \tag{8}$$

Suppose, then, that the launching and receiving antennae have similar electromagnetic properties, i.e. identical radiation patterns, with the latter positioned for collection with maximum efficiency of scattered waves from the first point. By replacing $\kappa_\perp$ with $k_0\alpha$ in the spectrum $G(\kappa_\perp)$, we obtain the collection efficiency of scattered waves from the second region

$$F = \exp\left(-\alpha^2/\alpha_0^2\right), \tag{9}$$

where $\alpha_0 = \Delta/k_0$. This, together with equation (8) and the Bragg condition, gives the instrumental selectivity function

$$F = \exp[-(2k\sin(\delta\varphi/2)/\Delta)^2], \tag{10}$$

where $k \approx k_0\theta$ is the wave number of detected fluctuations. In the case of a probing beam propagating perpendicularly to the magnetic surfaces, φ coincides with the magnetic pitch angle (apart from an additive constant) and equation (10) is equal to equation (4).

Finally, the polar angle φ can be obtained from equation (3), rewritten as

$$(\boldsymbol{k}_s - \boldsymbol{k}_0)\cdot\boldsymbol{B} = 0, \tag{11}$$

from which we get

$$B_t(\cos\theta - 1) + B_u\sin\,\theta\cos\,\varphi + B_v\sin\,\theta\sin\,\varphi = 0, \tag{12}$$

giving

$$\cos\,\varphi = \frac{B_u B_t\,(1 - \cos\,\theta) \pm \left[B_u^2 B_t^2(1 - \cos\,\theta)^2 - B_\perp^2\left(B_t^2(1 - \cos\,\theta)^2 - B_v^2\sin^2\,\theta\right)\right]^{1/2}}{B_\perp^2\sin\,\theta} \tag{13}$$

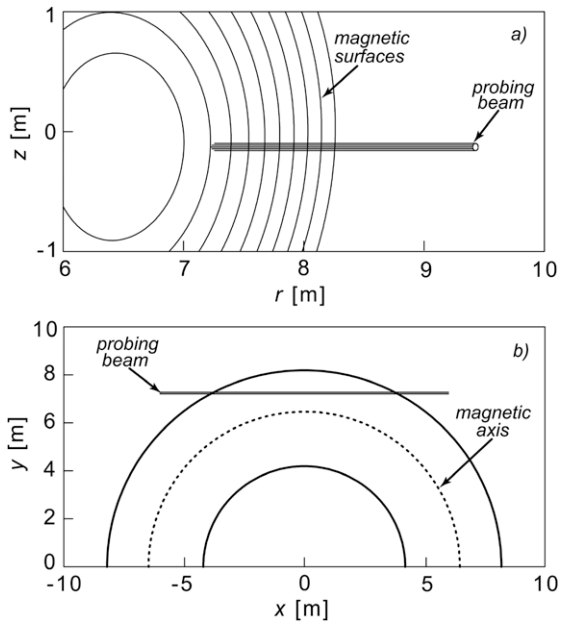

Figure 7. Poloidal (*a*) and toroidal (*b*) trajectories of a CO_2 Gaussian beam ($w = 3$ cm) propagating on the equatorial plane of the tokamak of figure 2 with a peak plasma density of 1×10^{20} m^{-3}.

and

$$\sin\varphi = \frac{B_t(1-\cos\theta) - B_u \sin\theta\cos\varphi}{B_v \sin\theta}, \tag{14}$$

where $B_\perp^2 = B_u^2 + B_v^2$ and with the $\pm$ sign corresponding to the two scattering branches of figure 5.

In the next section, these equations will be used for assessing the degree of localization of CO_2 laser scattering measurements in the next generation of burning plasma experiments. As a test-bed we will use the tokamak configuration of figure 2 with the official ITER parameters [2]: plasma major radius = 6.2 m, plasma minor radius = 2 m, toroidal magnetic field on axis = 5.3 T and plasma current = 15 MA.

4. CO_2 laser scattering

We begin with the scattering geometry of figure 7, where a probing beam with a frequency of 3×10^{13} Hz and a waist (w) of 3 cm propagates on the tokamak equatorial plane along the x-axis, and the scattering receiver is set for the measurement of fluctuations with wave vectors parallel to the equatorial plane. Here and in the following we will use the system of orthogonal coordinates (x, y, z) of figure 7, and we will refer to the plane containing the magnetic axis as the equatorial plane and to the (r–z) plane (with $r = \sqrt{x^2 + y^2}$) as the poloidal plane.

The beam ray trajectories, which in figure 7 are displayed on both equatorial and poloidal planes, are from a ray tracing code [15] including both wave refraction and first order diffraction effects. However, because of the large beam frequency, refractive effects are negligible. Furthermore, since $2x/k_0 w^2 \ll 1$, diffraction effects are negligible as well, and consequently the beam radius remains nearly constant and equal to w.

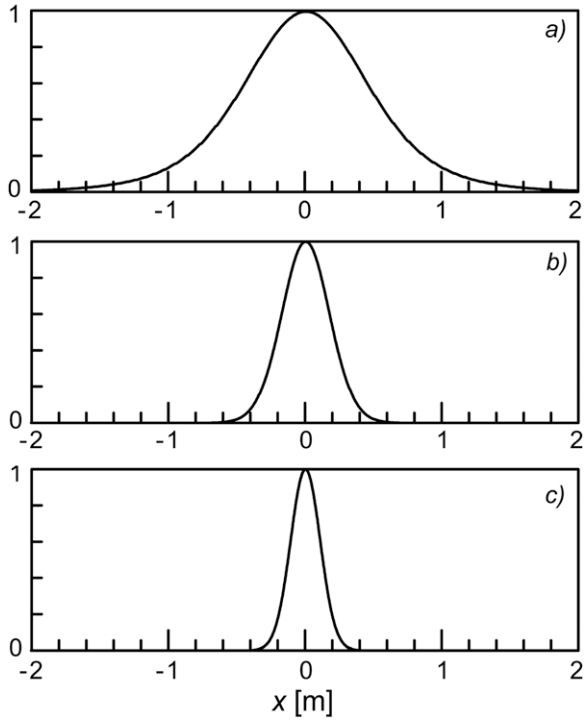

Figure 8. Instrumental selectivity function for the scattering geometry of figure 7 with $\varepsilon = 0.5$, $\beta = 14^\circ$ and (*a*) $k = 2\,\mathrm{cm}^{-1}$, (*b*) $k = 5\,\mathrm{cm}^{-1}$, (*c*) $k = 8\,\mathrm{cm}^{-1}$.

Since $\theta \ll 1$, the two scattering branches of figure 5 have similar selectivity functions with maxima near the point ($x = 0$, $y = y_0$), where y_0 is the initial y-coordinate of the probing beam. For simplicity, we will consider only the scattering branch corresponding to the + sign in equation (13). We will also refer to the quantity $\varepsilon = (y_0 - r_{\mathrm{ma}})/(y_{\mathrm{b}} - r_{\mathrm{ma}})$ (with y_{b} the maximum y-coordinate of the plasma boundary and r_{ma} the radius of the magnetic axis) as the normalized radius of the scattering region, and we will consider only cases with positive values of ε, i.e. with the scattering region on the low-field side of the torus.

Figure 8 shows the instrumental selectivity function along the central ray of the probing beam for $\varepsilon = 0.5 (y_0 = 7.4\,\mathrm{m})$ and three values of k. As expected from equation (10), the width of F (defined as the distance δx of the two points where $F = 1/e$) is a strongly decreasing function of k.

The corresponding components of $\boldsymbol{k}$ are displayed in figure 9, from which it appears that their relative amplitudes do not depend on the value of k. Indeed, this cannot be exactly true since $k_x = k^2/2k_0$ (equation (2)). However, since $k_x \approx 0$ because of the large k_0, the relative values of k_y and k_z are indeed insensitive to k. Finally, equations (2) and (3) make k_z (equal to zero at the peak of F, near $x = 0$) to grow towards the plasma boundary where, however, F is very small.

As shown in [14], the scattering region is located near the point where the angle between the probing wave vector and the magnetic field has its minimum value (β), with the width δx of F an increasing function of β. This can be easily understood by noting that in figure 5, β reaches its minimum value of $\theta/2$ near the magnetic axis, where the poloidal magnetic field is zero. Here, the width of the instrumental selectivity function is $\delta x \approx 2r_{\mathrm{ma}}\alpha_0 = 4r_{\mathrm{ma}}/k_0 w$,

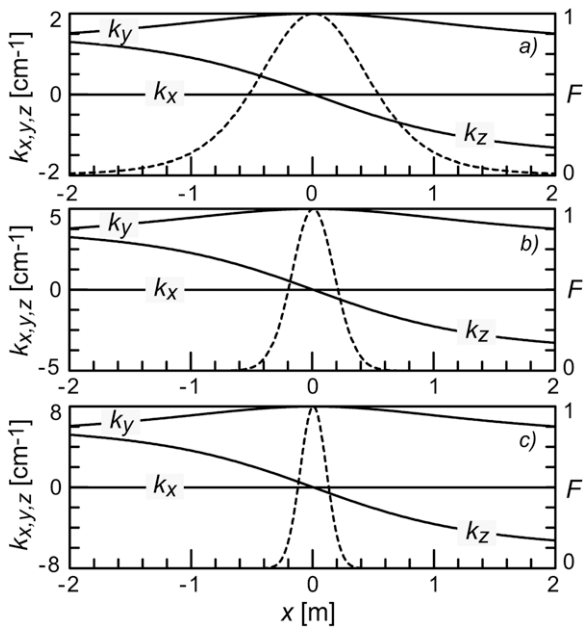

Figure 9. (x, y, z)-components of the wave vector $\boldsymbol{k}$ of detected fluctuations for the three cases in figure 8 (dashed lines are the instrumental selectivity functions).

which is much smaller than the values shown in figure 8 for $\beta = 14^\circ \gg \theta$. On the other hand, we have already seen that the selectivity function becomes very broad when $\beta = \pi/2$ (figure 4).

The strong dependence of F on β is illustrated in figure 10, showing that the width of F is a growing function of ε. Because of the magnetic pitch angle profile of figure 3, β is also a growing function of ε (going from 4.3° for $\varepsilon = 0.15$ to 18° for $\varepsilon = 0.7$). Hence, the conclusion that δx is an increasing function of β.

Another way of changing β is using a probing beam that propagates at an oblique angle with the equatorial plane, as in figure 11 where the beam is launched perpendicularly to the y-axis, as before, but now making an angle $\gamma = \pm 4.5^\circ$ with the x-axis (with $\pm$ indicating up-launching and down-launching, respectively). To emphasize the role of β, the launching points have been chosen to make the beam trajectory symmetric with respect to the equatorial plane. For $\varepsilon = 0.5$, this results in β varying from 9.5° for $\gamma = -4.5^\circ$ to 18.5° for $\gamma = +4.5^\circ$. The corresponding instrumental functions for $k = 2\,\mathrm{cm}^{-1}$ are in figure 12, showing a value of δx for $\gamma = +4.5^\circ$ that is more than twice that for $\gamma = -4.5^\circ$, again proving that the width of F is an increasing function of β. On the contrary, the F-weighted averages of the components of $\boldsymbol{k}$ (figure 13) are not very different and are similar to those for $\gamma = 0$ (figure 9(a)).

So far, we have considered the profile of the instrumental sensitivity function along the trajectory of the probing beam. Our results are summarized in figure 14, showing δx as a function of k for three radial positions. However, a crucial parameter of fluctuations measurements is their radial localization, which can be inferred from the distribution of F over the poloidal projection of the probing beam. More precisely, an estimate of the radial resolution can be obtained from the radial footprint (δr) of the set of points with $F > 1/e$, i.e. from $\delta r = \sqrt{(\delta x/2)^2 + y_0^2} - y_0$. This is displayed in figure 15, showing that δr becomes

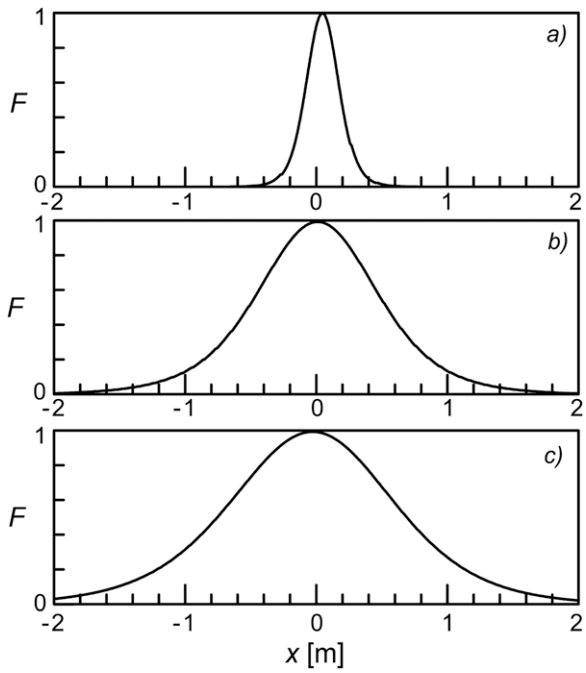

Figure 10. Instrumental function for the scattering geometry of figure 7 with $k = 2\,\mathrm{cm}^{-1}$ and (*a*) $\varepsilon = 0.15$ ($\beta = 4.3°$), (*b*) $\varepsilon = 0.5$ ($\beta = 14°$), (*c*) $\varepsilon = 0.7$ ($\beta = 18°$).

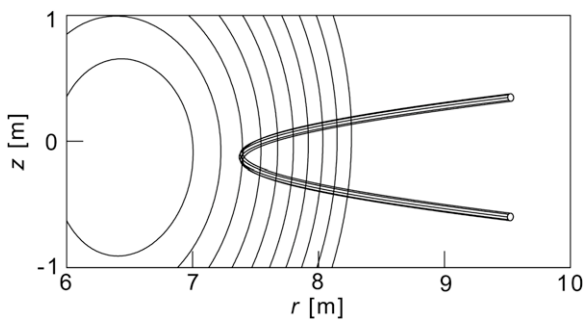

Figure 11. As in figure 7(*a*) with the probing beam making an angle of $\pm 4.5°$ with the x-axis. Initial points are chosen to make the beam trajectory symmetric with respect to the equatorial plane.

quickly much smaller than the beam diameter ($2w$) when $k > 2\,\mathrm{cm}^{-1}$. As noted above, because of a negligible wave refraction and diffraction, the beam radius is nearly constant and remains much smaller than any of the plasma scale lengths. Consequently, the results of figure 15 apply to all rays of the probing beam. Hence, the conclusion that the radial resolution of scattering measurements is essentially determined by the diameter of the probing beam.

5. Wave number resolution

The instrumental selectivity function used so far was defined in section 3 as the collection efficiency of waves scattered by fluctuations with the same value of k. In this section, we

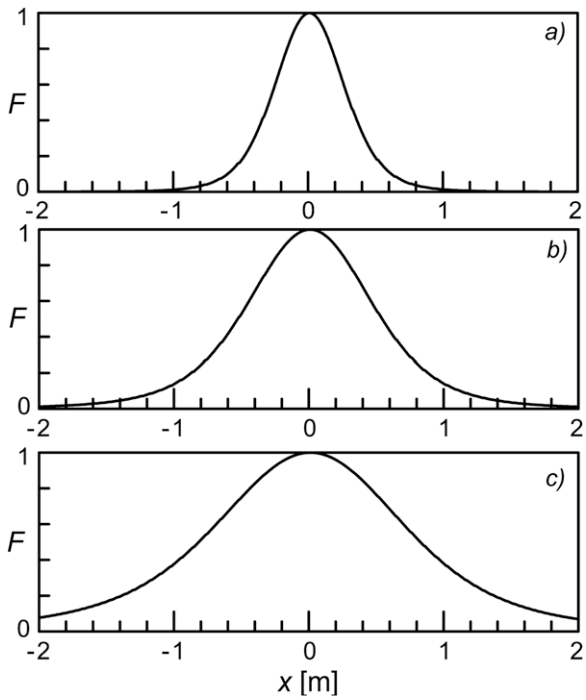

Figure 12. Instrumental function for $k = 2\,\mathrm{cm}^{-1}$, $\varepsilon = 0.5$ and (*a*) $\gamma = -4.5^\circ$ ($\beta = 9.5^\circ$), (*b*) $\gamma = 0^\circ$ ($\beta = 14^\circ$), (*c*) $\gamma = +4.5^\circ$ ($\beta = 18.5^\circ$).

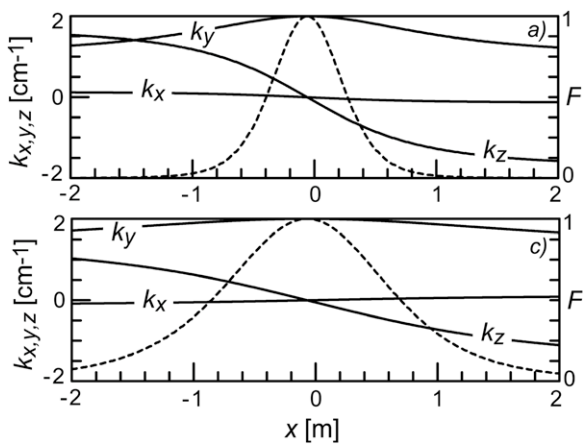

Figure 13. Same as in figure 9 for cases (*a*) [$\gamma = -4.5^\circ$, $\beta = 9.5^\circ$] and (*c*) [$\gamma = +4.5^\circ$, $\beta = 18.5^\circ$] of figure 12.

generalize the definition of selectivity function to include fluctuations with all possible wave numbers. To be more precise, let us consider again scattered waves originating from two points of the probing beam with wave vectors $\boldsymbol{k}_\mathrm{s}^1$ and $\boldsymbol{k}_\mathrm{s}^2$, respectively. From equation (5), we get

$$\frac{\boldsymbol{k}_\mathrm{s}^1 \cdot \boldsymbol{k}_\mathrm{s}^2}{\boldsymbol{k}_0 \cdot \boldsymbol{k}_0} \equiv \cos\,\alpha = \cos\,\theta_1 \cos\,\theta_2 + \sin\,\theta_1 \sin\,\theta_2\,(\cos\,\varphi_1 \cos\,\varphi_2 + \sin\,\varphi_1 \sin\,\varphi_2)\,, \tag{15}$$

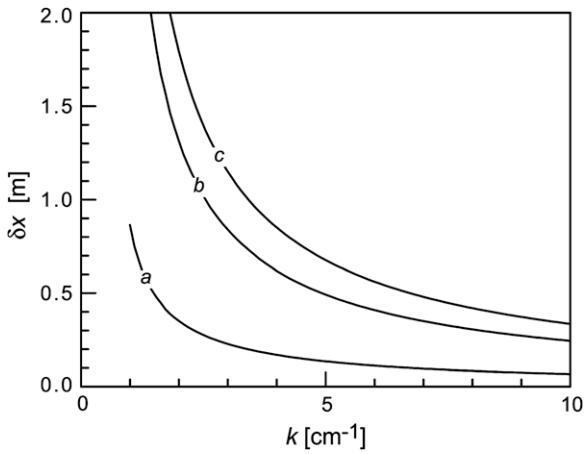

Figure 14. Width δx as a function of k along the central ray of a probing beam with $\gamma = 0^\circ$ and (a) $\varepsilon = 0.15$, (b) $\varepsilon = 0.50$, (c) $\varepsilon = 0.70$.

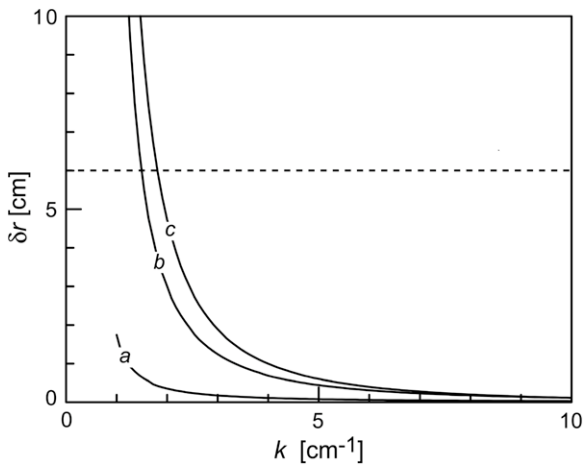

Figure 15. Radial footprint δr of the portion of central ray with $F > 1/e$ for the cases of figure 14. Dashed line represents the beam diameter ($2w$).

where θ_1 and θ_2 are the corresponding scattering angles. From this, we obtain

$$\cos\alpha = \cos(\theta_2 - \theta_1) - 2\sin\theta_1 \sin\theta_2 \sin^2(\delta\varphi/2), \tag{16}$$

where $\delta\varphi = \varphi_2 - \varphi_1$. Since both θ_1 and θ_2 are very small, this becomes

$$\alpha^2 \approx (\theta_2 - \theta_1)^2 + 4\theta_2\theta_1 \sin^2(\delta_\varphi/2). \tag{17}$$

The mismatch angle between $\boldsymbol{k}_s^1$ and $\boldsymbol{k}_s^2$ is made of two terms. The first, as expected, is due to the difference in scattering angles. The second, as before, is due to the spatial variation of magnetic pitch angles.

Following the same procedure that led to equation (10), we obtain a new expression for the instrumental selectivity function

$$G = \exp\left[-\left((k' - k)^2 + 4k'k\sin^2(\delta_\varphi/2)\right)/\Delta^2\right], \tag{18}$$

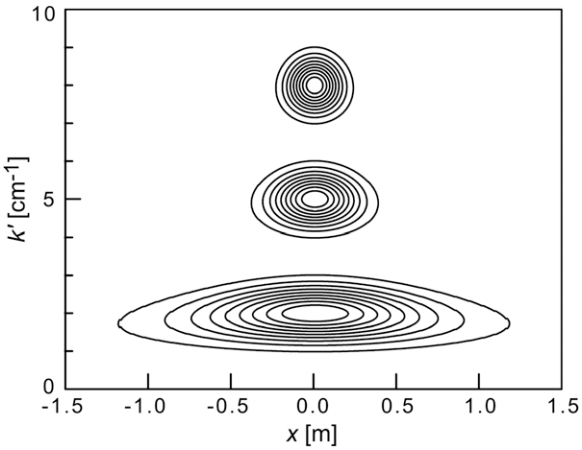

Figure 16. Contour plots (nine levels equally spaced from 0.1 to 0.9) of $G(k', x)$ for the three cases of figure 8.

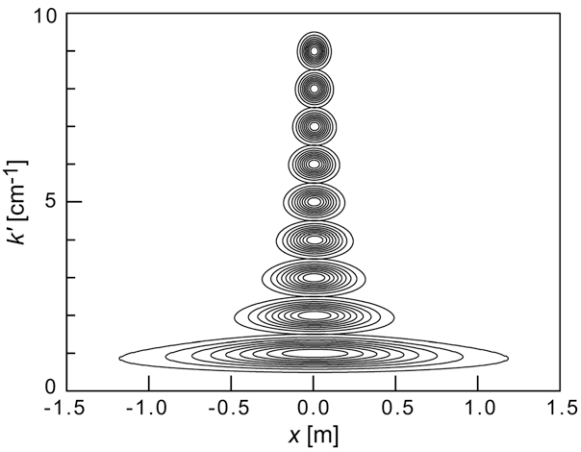

Figure 17. Contour plots (nine levels equally spaced from 0.1 to 0.9) of $G(k', x)$ for the scattering geometry of figure 7 with $\varepsilon = 0.5$, $w = 6\,\mathrm{cm}$ and $k = 1 - 9\,\mathrm{cm}^{-1}$ (from bottom to top).

where $k \approx k_0\theta_1$ is the tuning wave number of the receiver and $k' \approx k_0\theta_2$ is the wave number of detected fluctuations. For $k' = k$, we recover equation (10).

Contour plots of $G(k', x)$ are displayed in figure 16 for the same cases in figure 8. A comparison with the latter shows that the maximum width of G along the beam trajectory is similar to that of F. It also shows, as expected, that the wave number resolution remains $\approx \pm\Delta$.

Finally, the use of Gaussian beams—a crucial assumption in the scattering scheme of this paper—implies the availability of circular ports with substantially larger radii (r_w) than w. Assuming the conservative criterion of $r_w \approx 2w$, the value of w used so far (3 cm) would require ports that are much smaller than the size of ITER. Hence, we could envision using larger beams to obtain a substantial improvement in wave number resolution, as in figure 17 where the contour plots of $G(k', x)$ are displayed for $w = 6\,\mathrm{cm}$.

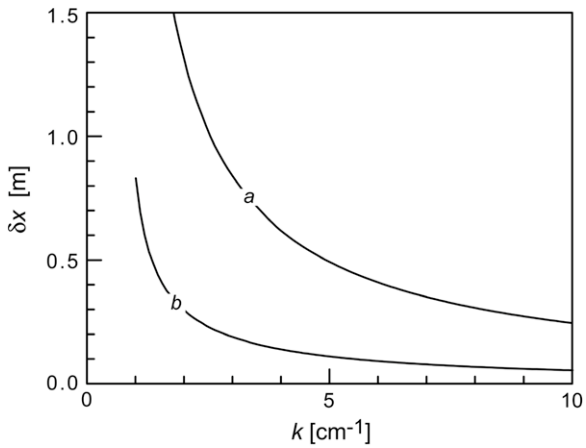

Figure 18. Width δx as a function of k for $\gamma = 0^\circ$ and $\varepsilon = 0.5$; (*a*) ITER, (*b*) IGNITOR.

6. Discussion

Throughout this paper, we have used an ITER-like plasma for deriving the properties of the proposed scattering scheme. However, since the instrumental sensitivity function depends only on the wave number of fluctuations, the radius and launching direction of the probing beam and the pitch angle of magnetic field lines, this scattering scheme will be capable of providing the same degree of spatial resolution in similar tokamaks. In other words, the ratio of δx to any of the plasma linear dimensions will be the same in tokamaks having identical aspect ratio, elongation, triangularity and magnetic safety factor. Indeed, since these quantities can vary only over a very narrow range of parameters, we may conclude that the advantages of the proposed scheme apply, mutatis mutandis, to any tokamak. This is demonstrated in figure 18, where the instrumental function for an IGNITOR-like plasma (major/minor radii $= 1.32/0.47$ m, toroidal magnetic field $= 13$ T, plasma current $= 12$ MA [1]) is compared with that for ITER, showing an ITER/IGNITOR ratio of 4.4 for δx, vis-à-vis one of 4.25 for the minor radii and 4.7 for the major radii (small discrepancy due to different aspect ratios, 3.1 versus 2.8).

As stated in the introduction, the benefits of CO_2 lasers stem from their high frequency and high power single-mode operation. However, since the instrumental selectivity function for a given value of k (equations (10) and (18)) does not depend on the frequency of the probing beam, the use of lower frequencies would preserve the localization properties of scattering measurements. As a matter of fact, a scattering apparatus based on the scheme described in this paper and employing a backward wave oscillator with a frequency of 2.8×10^{11} Hz is currently in use on NSTX for localized measurements of turbulent fluctuations driven by the ETG mode [16]. Obviously, the use of such a low probing frequency in a burning plasma experiment would defeat the spirit of this paper since both refractive and diffractive effects would become important. However, one could consider using other types of lasers, as for example those operating in the range of 3×10^{12} Hz (CH_3OH lasers).

Finally, it is worth noting that for the case of an ITER-like plasma the length of the scattering region along the probing beam (δx) will be much longer than in past CO_2 scattering measurements [4, 7]. Consequently, since the power of scattered waves varies like δx^2, we conclude that the use of the proposed scheme in an ITER-like plasma will allow the detection of smaller fluctuation levels than in previous CO_2 scattering measurements.

7. Conclusion

In summary, the results presented in this paper illustrate how the short-scale turbulence that plasma theory indicates as a potential cause of anomalous transport in the next generation of burning plasma experiments could be detected with good spatial and wave number resolution using coherent scattering of CO_2 lasers.

The unique feature of the proposed scheme is the oblique propagation of the probing wave with respect to the magnetic field, with the toroidal curvature of field lines playing a major role in improving the spatial resolution of measured signals. Furthermore, this scattering geometry has the additional advantage of reducing the footprint of the scattering region in the plasma radial direction. Finally, small scattering angles and negligible wave refraction effects minimize the size of needed ports—a matter of vital importance for a plasma diagnostic that must operate in the hostile environment of a burning plasma.

Acknowledgment

This work was supported by US DOE Contract No DE-AC02-76-CHO-3073.

References

[1] Coppi B, Nassi B and Sugiyama L E 1992 *Phys. Scr.* **45** 112
[2] 2001 *Technical Basis for the ITER Final Design* (*ITER EDA Documentation Series No 24*) (Vienna: IAEA)
[3] Horton W 1999 *Rev. Mod. Phys.* **71** 735
[4] Connor J W and Wilson H R 1994 *Plasma Phys. Control. Fusion* **36** 719
[5] Mazzucato E 1976 *Phys. Rev. Lett.* **36** 792
[6] Surko C M and Slusher R E 1976 *Phys. Rev. Lett.* **37** 1747
[7] Brower D L, Peebles W A and Luhmann N C Jr 1987 *Nucl. Fusion* **27** 2055
[8] Philipona R, Doyle E J, Luhmann N C Jr, Peebles W A, Rettig C, Burrell K H, Groebner R J, Matsumoto H and the DIII-D Group 1990 *Rev. Sci. Instrum.* **61** 3007
[9] Devynck P, Garbet X, Laviron C, Payan J, Saha S K, Gervais F, Hennequin P, Quéméneur A and Truc A 1993 *Plasma Phys. Control. Fusion* **35** 63
[10] Fonck R, Cosby G, Durst R D, Paul S F, Bretz N, Scott S, Synakowski E and Taylor G 1993 *Phys. Rev. Lett.* **70** 3736
[11] Mazzucato E and Nazikian R 1993 *Phys. Rev. Lett.* **71** 1840
[12] Mazzucato E 1998 *Rev. Sci. Instrum.* **69** 2201
[13] Rosenbluth M N and Rostoker N 1962 *Phys. Fluids* **5** 776
[14] Mazzucato E 2003 *Phys. Plasmas* **10** 753
[15] Mazzucato E 1989 *Phys. Fluids* B **1** 1855
[16] Smith D R, Mazzucato E, Munsat T, Park H, Johnson D, Lin L, Domier C W, Johnson M and Luhman N C Jr 2004 *Rev. Sci. Instrum.* **75** 3840